JOURNAL OF CATALYSIS 144, 148–159 (1993)

Catalytic Properties and Deactivation Behaviour of Crystalline Microporous MAPO-36

DEEPAK B. AKOLEKAR[1]

Department of Chemical Engineering, University of Laval, Ste-Foy, Quebec, Canada G1K 7P4

Received November 16, 1992; revised June 14, 1993

MAPO-36 showed high catalytic activity in conversion reactions of alcohols, linear, branched, and cycloalkanes, and aromatics. In ethanol, *n*-hexane, cyclohexane, and isooctane conversion reactions, MAPO-36 showed significantly higher conversion and concentration of aromatics than MAPO-5, SAPO-5, and $AlPO_4$-5. The distribution of aliphatics and aromatics is different in these reactions over MAPO-36, MAPO-5, SAPO-5, $AlPO_4$-5, and H-ZSM-5. MAPO-36 exhibited lower *n*-hexane conversion than H-ZSM-5; however, the aromatics yield was higher. The trend was reversed in the cyclohexane conversion reaction. The toluene disproportionation and *o*-xylene conversion activity of MAPO-36 is very high as compared to MAPO-5, SAPO-5, $AlPO_4$-5, and H-ZSM-5. In the *o*-xylene conversion reaction, MAPO-36 exhibited higher xylene loss, indicating that the disproportionation is more pronounced than the isomerization. The effect of pyridine-poisoned strong acid sites on the catalytic properties of the catalysts was studied. The influence of pulse number on the catalytic activity of MAPO-36 in *n*-pentane, *n*-hexane, 3-methylpentane, cyclohexane, methanol, and toluene reactions was investigated. The deactivation of MAPO-36 is lowest as compared to MAPO-5, SAPO-5, and $AlPO_4$-5 in the ethylbenzene conversion reaction. The results on the dependence of cumene cracking activity of MAPO-36, SAPO-5, and $AlPO_4$-5 on tine-on-stream show that the initial activity of MAPO-36 is high, though it decreases faster than that of SAPO-5 and $AlPO_4$-5. *In situ* IR techniques were used to investigate coke formation and temperature programmed oxidation of coke deposited during the cumene cracking reaction over MAPO-36.

INTRODUCTION

A novel crystalline microporous MAPO-36 material, a type of MeAPO molecular sieve family, was introduced by Flanigen *et al.* (*1*). MAPO-36 has a unique three-dimensional structure with monoclinic symmetry (*2*) and cell constants $a = 1.31$ nm, $b = 2.16$ nm, and $c = 0.52$ nm, $\beta = 92°$. The material is characterized by a 1-dimensional system of channels parallel to the *c*-axis with elliptical 12-ring apertures (pore diameter = 0.65×0.75 nm) and annular side pockets. The MAPO-36 framework is acidic and it possesses both Brønsted and Lewis acid sites (*3*).

Synthesis, characterization, acidity, and site energy distribution of this material were reported in earlier papers (*3, 4*). MAPO-36 shows higher *n*-butane cracking activity than other aluminophosphates (*5*) and also higher acidity than MAPO-5, SAPO-5, and $AlPO_4$-5 (*3*). The present investigation was undertaken in order to study the catalytic properties and deactivation/coking behaviour of MAPO-36 and to compare it with $AlPO_4$-5, SAPO-5, MAPO-5, and H-ZSM-5 catalysts under identical experimental conditions.

EXPERIMENTAL

Preparation of MAPO-36

Pr_3N-MAPO-36 was synthesized by hydrothermal crystallization of the gel ($1.8\ Pr_3N \cdot 0.17\ MgO \cdot 0.92\ Al_2O_3 \cdot 1.0\ P_2O_5 \cdot 40\ H_2O \cdot 0.33$ HOAc) initially at 378 K for 50 h

[1] Please address reprint requests to the author at the Department of Physical Chemistry, The University of New South Wales, P.O. Box 1, Kensington, NSW 2033, Australia.

0021-9517/93 $5.00

TABLE 1

Properties of MAPO-36, MAPO-5, SAPO-5, $AlPO_4$-5, and H–ZSM-5 Catalysts

Catalyst	Molar chemical composition	N_2 sorption capacity ($mmol \cdot g^{-1}$)	Crystal size (μm)	Crystal shape	Strong acid sites, q_i (673 K) ($mmol \cdot g^{-1}$)
MAPO-36	$0.17\ MgO \cdot 0.92\ Al_2O_3 \cdot 1\ P_2O_5$	5.56	11	H	0.0400
MAPO-5	$0.17\ MgO \cdot 0.92\ Al_2O_3 \cdot 1\ P_2O_5$	4.92	14	H	0.0065
SAPO-5	$0.17\ SiO_2 \cdot 1\ Al_2O_3 \cdot 0.92\ P_2O_5$	4.70	12	H	0.0054
$AlPO_4$-5	$1\ Al_2O_3 \cdot 1\ P_2O_5$	4.86	16	H	0.0025
H–ZSM-5	$1\ Al_2O_3 \cdot 61\ SiO_2$	5.00	4	PH	0.1800

Note. H, hexagonal rodlike; P, polyhedral.

and finally at 423 K for 24 h in a Teflon coated autoclave. The crystals of Pr_3N-MAPO-36 were thoroughly washed with deionized water, filtered, and dried in an air oven at 373 K for 16 h. The organic template was removed by calcination in the presence of air (flow 100 $cm^3 \cdot min^{-1}$) at 823 K for 20 h. The details of synthesis and characterization of MAPO-36 are given elsewhere (*4*).

The $AlPO_4$-5, SAPO-5, and MAPO-5 were prepared according to the procedure described by Wilson *et al.* (*6*). MAPO-36, MAPO-5, and SAPO-5 samples were prepared with similar concentrations of the substituted element (Mg/Si) in the aluminophosphate framework to compare their catalytic activity. H-ZSM-5 was obtained by deammoniating NH_4–ZSM-5 at 773 K in the presence of nitrogen (flow rate 100 $cm^3 \cdot min^{-1}$) for 8 h. The details of the preparation and characterization of the catalysts have been reported earlier (*4*, *7*). The product chemical composition, N_2-sorption capacity, morphology, and strong acid sites of these materials are reported in Table 1.

Measurement of Catalytic Activity

The catalytic activity of the catalysts in the alcohols-to-aromatics conversion and the linear, branched, and cycloalkanes and aromatic hydrocarbons conversion reactions have been determined in a pulse microreactor (i.d. 4 mm) connected to a gas chromatograph. The reaction conditions are given in the respective tables and figures. Before the activity was measured, the catalyst was heated at 673 K for 1 h in a flow of helium. The details of the microreactor and the experimental procedures for measuring the catalytic activity and for the selective poisoning of the catalysts were reported earlier (*7*, *8*). In order to compare MAPO-36, MAPO-5, SAPO-5, $AlPO_4$-5, and H-ZSM-5 for their deactivation due to coke deposition, the conversion of ethylbenzene was measured as a function of pulse number.

The catalytic activity and deactivation/coking behaviour of MAPO-36, SAPO-5, and $AlPO_4$-5 in cumene cracking as a function of time-on-stream were investigated using IR and GC techniques. The investigations were performed using self-supported wafers 15 mg, thickness 10.0 $mg \cdot cm^{-2}$. Prior to the reaction, the catalyst was activated *in situ* at 773 K for 5 h in the presence of helium. Cumene reaction was carried out by passing the vapours (P_{cumene}: 8.93 mbar) along with helium (flow rate 60 $cm^3 \cdot min^{-1}$) over the catalyst at 673 K. The reaction products were analyzed simultaneously by on-line GC. The *in situ* IR spectrum was recorded to investigate the deactivation of MAPO-36. The schematic and details of the experimental set-up for the *in situ* IR and the conversion measurements of cumene cracking in the *IR*–microreactor flow cell were reported earlier (*9*, *10*). The deactivated MAPO-36 was regenerated at 825 K

TABLE 2

Ethanol Conversion over MAPO-36, MAPO-5, SAPO-5, $AlPO_4$-5, and H–ZSM-5 at 673 K

Catalyst	MAPO-36	MAPO-5	SAPO-5	$AlPO_4$-5	H–ZSM-5
Conversion (%)	74.0	62.6	53.0	30.0	78.0
Aromatics concentration (wt%)	4.1	0.6	0.3	0.1	10.5
Product distribution (wt%)					
Methane	0.1	0.2	—	—	0.4
Ethane	21.0	6.8	3.7	1	20.2
Ethene	40.6	88.1	93.7	97.8	21.0
Propane	6.0	0.4	0.8	0.2	8.4
Propene	1.1	0.8	0.4	0.1	1.1
Butanes	7.2	0.3	0.4	0.2	15.5
Butene	0.8	—	0.2	0.1	0.9
C_5^+-aliphatics	17.7	2.4	0.2	0.2	15.5
Aromatics	5.5	1.0	0.6	0.3	13.5
Total	100	100	100	100	100
Aromatics distribution (wt%)					
Benzene	7.3	2.0			13.5
Toluene	31.7	6.0			44.5
Ethylbenzene	—	—			3.4
Xylenes	39.0	18.8			24.3
Trimethylbenzenes	9.8	20.0			9.3
Other C_9^+-aromatics	12.2	54.2			5.0
Total	100	100			100
p-X/*m*-X	0.92	0.88			1.13
p-x/*o*-X	0.86	0.83			1.07
Selectivity for xylenes (%)	2.2	0.3			3.4

Note. Reaction conditions: amount of catalyst 0.045 g; He flow rate 90 $cm^3 \cdot min^{-1}$; pulse size 5 μl.

in the flow of a mixture of helium and oxygen (20%) for 5 h.

MAPO-36 was coked by passing cumene vapours (P_{cumene}: 8.93 mbar) along with helium (flow rate 60 $cm^3 \cdot min^{-1}$) at 673 K for 24 h. Temperature programmed oxidation of coke was carried out in the presence of a mixture of helium and oxygen (20%) (total flow 60 $cm^3 \cdot min^{-1}$, temperature range 450 to 875 K, heating rate 10 $K \cdot min^{-1}$).

RESULTS AND DISCUSSION

Table 1 shows the properties of MAPO-36, MAPO-5, SAPO-5, $AlPO_4$-5, and H-ZSM-5. Morphological investigations indicated high crystallinity of the catalysts. The N_2-sorption capacity of MAPO-36 is higher than those of MAPO-5, SAPO-5, and $AlPO_4$-5. This result is similar to one already reported (*5*). The order of strong acid sites over the catalysts is as follows: H-ZSM-5 $\gg$ MAPO-36 $\gg$ MAPO-5 > SAPO-5 > $AlPO_4$-5.

In Table 2, the results of ethanol conversion over MAPO-36 are compared to similar results obtained with H-ZSM-5, MAPO-5, SAPO-5, and $AlPO_4$-5. In the ethanol conversion reaction, MAPO-36 showed higher conversion and concentration of aromatics formation as compared with MAPO-5, SAPO-5, and $AlPO_4$-5. This is attributed to the presence of more strong acid sites on MAPO-36. The observed order of catalytic activity and aromatics selectivity is same as the order found for strong acid sites. Our earlier investigation (*3*) on the acidity and acid strength distribution on these materials indicated that the concentration of Brønsted acid sites is higher on MAPO-36. Also, temperature programmed desorption and step-

wise thermal desorption of pyridine over these materials showed that the amount of pyridine chemisorbed on MAPO-36 above 673 K was significantly higher, indicating the presence of stronger acidic sites. The observed conversion changes are accompanied by parallel changes in the product distribution, a higher activity yielding more aromatics and less C_1 to C_5 aliphatics.

The aliphatics distribution in the ethanol conversion reaction is quite different among the catalysts. MAPO-36 showed lower ethene formation and higher ethane, propane, propene, butane, and C_5--aliphatics formation as compared to MAPO-5, SAPO-5, and $AlPO_4$-5. Comparison of the aliphatics distribution over H-ZSM-5 and MAPO-36 indicated that ethene and C_5--aliphatics formation was higher over MAPO-36.

The distribution of the aromatics formed on MAPO-36, MAPO-5, SAPO-5, $AlPO_4$-5, and H-ZSM-5 is quite different. MAPO-36 shows higher benzene, toluene, and xylene formation and also paraselectivity than MAPO-5, SAPO-5 and $AlPO_4$-5. The amounts of benzene and toluene formed, the selectivity for *p*-xylene, *p*-X/*m*-X (*p*-Xylene/*m*-Xylene) and *p*-X/*o*-X ratios were all higher in H-ZSM-5. The formation of C_9--aromatics in ethanol conversion reaction is higher on the aluminophosphate catalysts. The observed higher C_9--aromatics in the aluminophosphates is due to their large pore diameter and decreased degree of pore constraint unlike H-ZSM-5 (*11–13*). In the case of H-ZSM-5, the lower formation of C_9--aromatics can be explained in terms of the higher spatial constraints on the reaction, in spite of the stronger acidity. The large differences in the acidity and channel structure of the aluminophosphates and pentasil zeolite are responsible for the different distribution of aromatics in ethanol conversion. Due to the lower acidity of MAPO-36 and MAPO-5 (compared to H-ZSM-5), alkylation of the lower aromatics is favoured over dealkylation of the higher aromatics.

The decrease in the conversion and aromatics concentration in the reaction of methanol over MAPO-36 as a function of pulse number are presented in Figs. 1 and 2, respectively. In the first pulse experiment of methanol to aromatics, an aromatics concentration of 23.1 wt% was observed. The aromatics formation decreases with the pulse number. The results of methanol-to-aromatics conversion as a function of pulse number over MAPO-36, H-ZSM-8 (*7*) and $AlPO_4$-5 (*7*) indicated more pronounced decrease in the aromatics formation over MAPO-36 compared to H-ZSM-8. In the

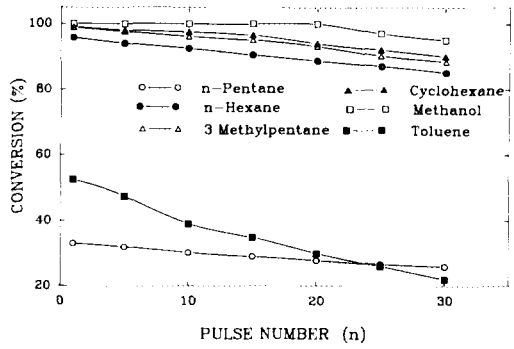

FIG. 1. Influence of the pulse number on the total conversion of aliphatic and aromatic hydrocarbons and alcohols on MAPO-36. Reaction conditions: amount of catalyst 0.100 g; He flow rate 30 $cm^3 \cdot min^{-1}$; total pressure 270 kPa; temperature 673 K; pulse size 1 μl).

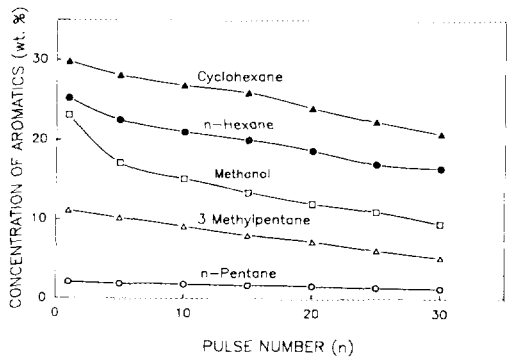

FIG. 2. Formation of aromatics in the conversion of aliphatic hydrocarbons and alcohol over MAPO-36. Reaction conditions: amount of catalyst 0.100 g; He flow rate 30 $cm^3 \cdot min^{-1}$; total pressure 270 kPa; temperature 673 K; pulse size 1 μl.)

TABLE 3

Conversion of *n*-Hexane over MAPO-36, MAPO-5, SAPO-5, $AlPO_4$-5, and H–ZSM-5 at 673 K

Catalyst	MAPO-36	MAPO-5	SAPO-5	$AlPO_4$-5	H–ZSM-5
Conversion (%)	33.8	1.8	1.0	0.3	41.6
Aromatics concentration (wt%)	10.7	0.8	0.4	<0.04	4.0
Product distribution (wt%)					
Methane	1.8	—	2.0		4.3
Ethane	25.6	22.2	20.0		40.4
Ethene	2.4	5.5	2.0		7.7
Propane	17.2	11.1	23		23.6
Propene	0.9	—	—		1.4
Butanes	11.2	11.2	10.0		4.3
Butene	0.6	—	—		1.0
C_5-aliphatics	8.6	5.6	3.0		7.7
Aromatics	31.7	44.4	40.0		9.6
Total	100	100	100		100
Aromatics distribution (wt%)					
Benzene	0.9	6.3	10.0		7.5
Toluene	3.7	12.5	20.0		32.5
Ethylbenzene	0.9	6.2	—		2.5
Xylenes	24.3	37.5	50.0		22.5
Trimethylbenzenes	20.6	18.8	13.0		12.5
Other C_9-aliphatics	49.7	18.7	7.0		22.5
Total	100	100	100		100

Note. Reaction conditions: amount of catalyst 0.045 g; He flow rate 90 $cm^3 \cdot min^{-1}$; pulse size 5 μl.

20th pulse experiment, the extent of decrease in the aromatics formation is as follows: MAPO-36 54%, H-ZSM-8 < 3%, and $AlPO_4$-5 80%.

The results in Tables 3–5 indicate that the catalytic activity of the catalysts varies in *n*-hexane, cyclohexane, and isooctane reactions. In *n*-hexane, cyclohexane, and isooctane conversion reactions, MAPO-36 showed higher catalytic activity and aromatics formation than MAPO-5, SAPO-5 and $AlPO_4$-5. Comparing the results of *n*-hexane conversion over H-ZSM-5 and MAPO-36, it is observed that the *n*-hexane conversion is lower over MAPO-36; however, the aromatics formation is higher. It is interesting to note that the aliphatics and aromatics distributions in *n*-hexane, cyclohexane, and isooctane reactions over the catalysts are different (Tables 3–5). The order of catalytic activity and aromatics formation in *n*-hexane, cyclohexane, and isooctane reactions are presented in Table 6. In the *n*-hexane reaction, the formation of xylenes, trimethylbenzenes, and other C_9+-aromatics was greater on MAPO-36, while toluene formation was greater over H-ZSM-5. The catalytic activity of MAPO-36 in the cyclohexane reaction was higher than that of H-ZSM-5; however, the concentration of aromatics formed was lower. The formation of various alphatic and aromatic products occurs due to the cracking of cyclohexane; further, the cracked products are aromatized over the catalyst depending upon its acidity. Haung and Kaliaguine (*14*) reported that the cyclohexane conversion reaction over H-ZSM-5 goes through cracking and further aromatization rather than dehydrogenation.

In the isooctane conversion reaction over the catalysts, MAPO-36 shows significant activity and higher aromatics formation. The larger pore opening of MAPO-36 and the type 5 aluminophosphates is responsible for the higher conversion of isooctane as compared to H-ZSM-5. The results are consistent with earlier studies (*15*) in which the large pore zeolites (HM, HY) showed very

TABLE 4

Conversion of Cyclohexane over MAPO-36, MAPO-5, SAPO-5, $AlPO_4$-5, and H–ZSM-5 at 673 K

Catalyst	MAPO-36	MAPO-5	SAPO-5	$AlPO_4$-5	H–ZSM-5
Conversion (%)	34.4	8.7	1.6	0.6	28.9
Aromatics concentration (wt%)	8.5	1.0	0.4	<0.05	11.0
Product distribution (wt%)					
Methane	1.8	1.1	0.5		3.5
Ethane	21.6	5.7	6.9		30.8
Ethene	0.3	1.2	0.4		5.2
Propane	15.2	6.9	12.0		14.2
Propene	0.3	1.0	0.6		1.0
Butanes	11.6	3.4	4.0		1.7
Butene	0.3	1.1	0.9		0.3
C_5^+-aliphatics	23.0	68.1	49.7		5.3
Aromatics	25.9	11.5	25		38.0
Total	100	100	100		100
Aromatics distribution (wt%)					
Benzene	2.4	5.0			1.0
Toluene	22.4	20.0			24.5
Ethylbenzene	2.7	5.0			3.6
Xylenes	34.2	30.0			28.2
Trimethylbenzenes	20.0	20.0			10.9
Other C_9^+-aromatics	18.3	20.0			31.8
Total	100	100			100

Note. Reaction conditions: amount of catalyst 0.045 g; He flow rate 90 $cm^3 \cdot min^{-1}$; pulse size 5 μl.

TABLE 5

Conversion of Isooctane over MAPO-36, MAPO-5, SAPO-5, $AlPO_4$-5, and H–ZSM-5 at 673 K

Catalyst	MAPO-36	MAPO-5	SAPO-5	$AlPO_4$-5	H–ZSM-5
Conversion (%)	32.9	26.2	1.8	0.5	0.3
Aromatics concentration (wt%)	3.0	1.4	0.8	<0.1	
Product distribution (wt%)					
Methane	1.5	0.7	2.0		
Ethane	18.8	7.8	14.0		
Ethene	0.3	0.7	0.6		
Propane	40.4	65.7	15.5		
Propene	0.3	0.7	0.2		
Butanes	19.9	3.7	16.0		
Butene	0.3	0.4	0.2		
C_5^+-aliphatics	9.4	15.1	7.1		
Aromatics	9.1	5.2	44.4		
Total	100	100	100		
Aromatics distribution (wt%)					
Benzene	4.0	3.6	12.5		
Toluene	24	14.3	25.0		
Ethylbenzene	—	1.4	—		
Xylenes	38.7	55.7	37.5		
Trimethylbenzenes	16.6	17.9	12.5		
Other C_9^+-aromatics	16.7	7.1	12.5		
Total	100	100	100		

Note. Reaction conditions: amount of catalyst 0.045 g; He flow rate 90 $cm^3 \cdot min^{-1}$; pulse size 5 μl.

TABLE 6

Order of Catalytic Activity and Extent of Aromatics Formation in *n*-Hexane, Cyclohexane, and Isooctane Reactions over the Catalysts

	Catalytic activity
n-Hexane:	H–ZSM-5 > MAPO-36 ≫ MAPO-5 > SAPO-5 > $AlPO_4$-5
Cyclohexane:	MAPO-36 > H–ZSM-5 ≫ MAPO-5 ≫ SAPO-5 > $AlPO_4$-5
Isooctane:	MAPO-36 > MAPO-5 ≫ SAPO-5 > $AlPO_4$-5 > H–ZSM-5
	Aromatics formation
n-Hexane:	MAPO-36 ≫ H–ZSM-5 ≫ MAPO-5 > SAPO-5 ≫ $AlPO_4$5
Cyclohexane:	H–ZSM-5 > MAPO-36 ≫ MAPO-5 > SAPO-5 ≫ $AlPO_4$-5
Isooctane:	MAPO-36 ≫ MAPO-5 > SAPO-5 > $AlPO_4$-5

high isooctane cracking activity than the pentasil zeolites. The higher conversion of *n*-hexane, cyclohexane, and isooctane and the concentration of aromatics formation in these reactions over MAPO-36 is attributed to the higher acidity.

Figures 1 and 2 show the results of the conversion of *n*-pentane, *n*-hexane, 3-methylpentane, and cyclohexane and the concentration of aromatics in the hydrocarbons formed in these reactions on MAPO-36 at 673 K as a function of pulse number. MAPO-36 activity (in the first pulse experiment) in the conversion of *n*-hexane, 3-methylpentane, and cyclohexane is higher than in the conversion of *n*-pentane. The hydrocarbons conversion decreases with the pulse number. The catalytic activity order in the hydrocarbon cracking is as follows: cyclohexane > 3-methylpentane > *n*-hexane ≫ *n*-pentane. The sequence in the extent of aromatization in the hydrocarbons reactions is as follows: Cyclohexane > *n*-Hexane > 3-Methyl pentane > *n*-Pentane.

The product distribution in toluene disproportionation on the unpoisoned and pyridine poisoned catalysts at 673 K is given in Table 7. In the toluene disproportionation reaction over the catalysts, MAPO-36 exhibited higher catalytic activity, however, the xylene selectivity was found to be lower

TABLE 7

Product Distribution in Toluene Disproportionation on the Unpoisoned and Pyridine-Poisoned MAPO-36, MAPO-5, SAPO-5, $AlPO_4$-5, and H–ZSM-5 at 673 K

Catalyst	MAPO-36		MAPO-5		SAPO-5		$AlPO_4$-5		H–ZSM-5	
	U	P	U	P	U	P	U	P	U	P
Convn. (%)	52.4	1.4	5.0	0.7	3.5	1.2	0.6	0.3	12.3	0.9
Product distribution (wt%)										
Aliphatics	1.5	—	0.1	—	0.1	—	—	—	0.1	—
Benzene	23.5	0.2	1.5	0.4	1.3	0.1	0.1	0.1	5.8	0.3
Toluene	47.6	98.6	95.0	99.3	96.5	98.8	99.4	99.7	87.7	99.1
p-Xylene	7.5	0.2	0.6	—	0.5	0.2	0.1	0.1	2.0	0.2
m-Xylene	9.0	0.1	0.8	—	0.5	0.2	0.1	—	2.6	0.2
o-Xylene	5.1	0.1	0.3	—	0.3	0.1	0.1	—	1.2	0.1
C_9^+-aromatics	5.3	0.8	1.7	0.3	0.8	0.6	0.2	0.1	0.6	0.1
Total	100	100	100	100	100	100	100	100	100	100
Selectivity for Xylenes (%)	41.2	40.0	34	—	37.1	50	50	33	47.2	55.6
B/X	1.1	0.5	0.9	—	1.0	0.7	0.3	1.0	1.0	1.0
p-X/*m*-X	0.8	2.0	0.75	—	1.0	1.0	1.0	—	0.8	1.0
p-X/*o*-X	1.5	2.0	2.0	—	1.7	2.0	1.0	—	1.7	2.0

Note. Reaction conditions: amount of catalyst 0.100 g; He flow rate 30 $cm^3 \cdot min^{-1}$; pulse size 1 μl. U: unpoisoned; P: pyridine poisoned; B/X: Benzene/Total xylenes.

TABLE 8

Conversion of *o*-Xylene over MAPO-36, MAPO-5, SAPO-5, $AlPO_4$-5, and H–ZSM-5 at 673 K

Catalyst	MAPO-36	MAPO-5	SAPO-5	$AlPO_4$-5	H–ZSM-5
Conversion (%)	71.1	63.8	4.0	1.2	39.3
Product distribution (wt%)					
Aliphatics	0.5	0.2	0.1	—	0.4
Benzene	0.8	0.5	0.2	0.1	0.4
Toluene	7.3	3.5	0.4	0.1	1.3
p-Xylene	22.4	23.0	1.4	0.3	17
m-Xylene	29.0	30.5	1.7	0.4	19
o-Xylene	28.9	36.2	96.0	98.0	60.7
Trimethylbenzenes	9.7	5.6	0.2	0.2	0.2
Other C_{9^+}-aromatics	1.9	0.3	—	—	1.0
Total	100	100	100	100	100
Xylene loss (wt%)	19.7	10.3	0.9	0.4	3.3
Selectivity for *p*- and *m*-xylenes	72.3	83.9	77.0	63.6	91.6
Benzene/toluene	0.10	0.14	0.5	1.0	0.03
p-X/*m*-X	0.77	0.75	0.87	0.75	0.89

Note. Reaction conditions: amount of catalyst 0.045 g; He flow rate 90 $cm^3 \cdot min^{-1}$; pulse size 5 μl.

than that of H-ZSM-5 by 42.4%. The high toluene disproportionation activity of MAPO-36 as compared with the aluminophosphates of type 5 is due to the presence of a higher number of strong acid sites (*3*). The results of product distribution show that the formation of xylenes and C_{9^+}-aromatics is greater over MAPO-36. The low disproportionation activity of H-ZSM-5 is due to its intermediate shape selectivity regardless of the higher acidity than that of MAPO-36. Figure 1 shows the decrease in toluene disproportionation activity of MAPO-36 as a function of pulse number. With the pulse number, the catalytic activity of MAPO-36 decreases continuously and at the 30th pulse the total toluene conversion is reduced by 58%. After regeneration of the deactivated MAPO-36 in the presence of helium and oxygen (7%) mixture at 783 K for 14 h, the initial activity was 97% restored.

Selective poisoning of the stronger acid sites of MAPO-36 and other catalysts with pyridine (Table 7) shows that the catalytic activity in the toluene disproportionation is decreased, which indicates involvement of stronger acid sites (*16*). Also, the poisoning of the external acid sites (particularly, those located near pore openings) affects the diffusion of reactant molecules through the pores so that their interaction with the acid sites localized within the pores is reduced. This in part causes the decrease in the catalytic activity. Poisoning of MAPO-36 and other catalysts showed a strong influence on *p*-X/*m*-X and *p*-X/*o*-X ratios; poisoning caused marked increase in these ratios. The increase in the *para* isomer is expected mostly because of the increase in diffusional resistance in the aluminophosphates and the zeolite resulting from the blockage of a fraction of a pathways in the volume or at the boundary of the catalyst crystals (*17*). Also, a decrease in the diffusivity of the zeolite due to poisoning is commonly observed (*18*).

MAPO-36 showed higher catalytic activity in *o*-xylene conversion reaction (Table 8) and formation of more benzene, toluene, trimethylbenzenes, and other C_{9^+}-aromatics. Also, the xylene loss (which reflects the selectivity for isomerization in the *o*-xylene conversion) is highest for MAPO-36. This indicates that the disproportionation is more pronounced than the isomerization in the *o*-xylene conversion reaction over MAPO-36.

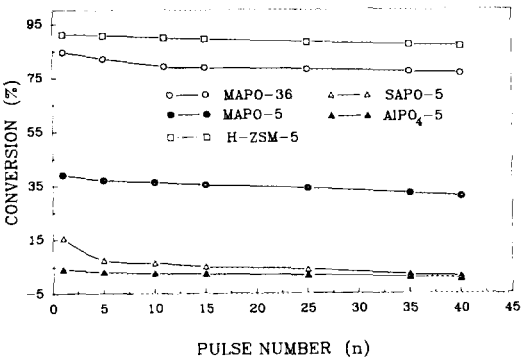

FIG. 3. Effect of the pulse number on the conversion of ethylbenzene on the catalysts. Reaction conditions: amount of catalyst 0.100 g; He flow rate 30 $cm^3 \cdot min^{-1}$; total pressure 270 kPa; temperature 673 K; pulse size 1 μl.

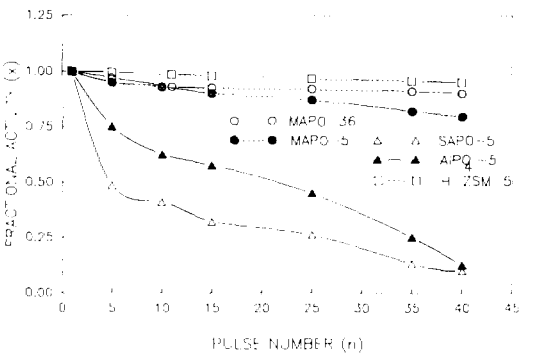

FIG. 4. Effect of the pulse number on the fractional catalytic activity of the catalysts in the conversion of ethylbenzene.

The decrease in conversion and aromatics formation in the *n*-pentane, *n*-hexane, 3-methylpentane, cyclohexane, methanol, and toluene conversion reactions over MAPO-36 with the pulse number (Figs. 1 and 2) are due to deactivation of acid sites or pore blockage by carbonaceous products. In methanol-to-aromatics conversion, the decrease in the concentration of aromatics is more pronounced than for the aliphatic hydrocarbons.

Figure 3 shows the results of ethylbenzene conversion on the catalysts at 673 K. The conversion of ethylbenzene (in the first pulse experiment) on MAPO-36 is very close to that of H-ZSM-5 and substantially higher than MAPO-5, SAPO-5, and $AlPO_4$-5. The influence of pulse number on fractional ethylbenzene activity (x) (where x = (conversion of ethylbenzene for a particular pulse)/(conversion of ethylbenzene for the first pulse)) of MAPO-36 and the other catalysts shown in Fig. 4 represents the deactivation trends. The deactivation of MAPO-36 is less pronounced than that of MAPO-5, SAPO-5, and $AlPO_4$-5 but higher than that of H-ZSM-5. The order of deactivation of the catalysts in the 40th pulse is SAPO-5 > $AlPO_4$-5 > MAPO-5 > MAPO-36 > H-ZSM-5. The deactivation trend of the large pore aluminophosphates (types 5 and 36) is similar to that of the large pore zeolites (HM, HX, HY) (*15*, *19*) with respect to the pentasil zeolites. The lower deactivation rate of MAPO-36 than of the type 5 aluminophosphates is due to its smaller pore size and typical structure.

Time-on-stream cumene cracking of MAPO-36, SAPO-5, and $AlPO_4$-5 is shown in Fig. 5. MAPO-36 shows higher cumene cracking activity than SAPO-5 and $AlPO_4$-5, which is due to the presence of stronger acid sites. The dependence of cumene cracking activity of MAPO-36, SAPO-5, and $AlPO_4$-5 on time-on-stream is shown in Fig. 5. A comparison of the results show that the overall decrease in cumene cracking activity of MAPO-36 with time-on-stream is much

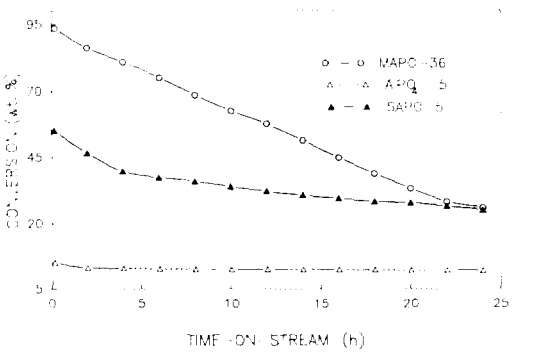

FIG. 5. Catalytic activity of MAPO-36, SAPO-5, and $AlPO_4$-5 in the cracking of cumene as a function of time-on-stream.

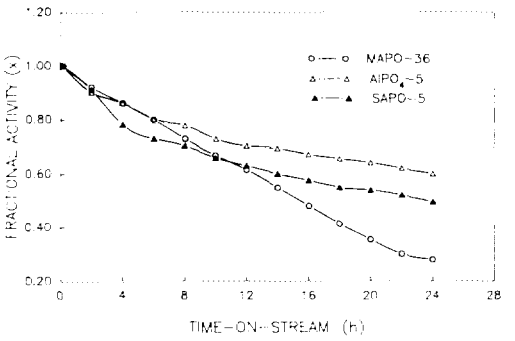

FIG. 6. Variation in the fractional catalytic activity of MAPO-36, SAPO-5, and $AlPO_4$–5 in the cumene cracking with time-on-stream.

steeper than that of SAPO-5 and $AlPO_4$-5. The faster deactivation of MAPO-36 is due to the high acidity. Cumene conversion and formation of carbonaceous products (coke) are increased due to higher acidity. The slow deactivation of $AlPO_4$-5 is attributed to its weak acidity and lower catalytic activity (*7, 19*). The initial rate of deactivation of MAPO-36 (Fig. 6) is similar to that of $AlPO_4$-5 up to 6 h of time-on-stream but lower than SAPO-5. The rate of deactivation of MAPO-36 is higher than that of SAPO-5 after 11 h of time-on-stream. The total decrease in the catalytic activity of MAPO-36 in the period of 24 h time-on-stream is 72%, while in the case of SAPO-5 and $AlPO_4$-5 it is 50% and 40%, respectively. The sharp decrease in the cumene cracking activity of MAPO-36 (large pore aluminophosphates with unidimensional pore system) with time-on-stream is due to the deactivation of the active acid sites and pore mouth blockage of the aluminophosphate by coke deposition. Due to coke deposition at the entrance of its unidimensional channels, the inner active acid sites are inaccessible to reactants.

Micropore volume measurements of the coked MAPO-36 by the BET method showed decrease in the micropore volume by 12.8% and an increase in the meso- and macropore volume by 48.8% (i.e., pore volume above 10 Å radius). The volume of micropores occupied by coke, calculated from the uncoked and coked MAPO-36, is 0.021 $cm^3 \cdot g^{-1}$. Increase in the meso- and macropore volume of coked MAPO-36 indicates that a certain amount of coke is deposited on the external surface of the crystallites. The thermogravimetric analysis of the coked sample showed 6.3% coke deposition over MAPO-36.

The cumene cracking activity of the regenerated MAPO-36 was regained to a large extent (97%). The large recovery in the catalytic activity of MAPO-36 reveals that the deactivation is due to blockage of the channels by strongly sorbed or occluded large hydrocarbons molecules. The remaining 3% loss in catalytic activity of the regenerated MAPO-36 is due to the deactivation of some of the strong acid sites by strongly sorbed carbonaceous species. This shows that the removal of strongly sorbed carbonaceous species is difficult at the regeneration temperature of 825 K.

Coke formation studies on MAPO-36 were carried out by a cumene cracking reaction at 675 K using *in situ* IR measurements. The extent of coke formation during the cumene cracking reaction was measured by the absorbance band at around 1585 cm^{-1} (Fig. 7). After 30 min of the cumene reaction, the coke formed over MAPO-36 evidenced by an increase in the so-called coke band at 1585 cm^{-1}. The 1585 cm^{-1} band is assigned to the C=C stretching vibrations in polyalkenes and/or aromatics (*20–22*).

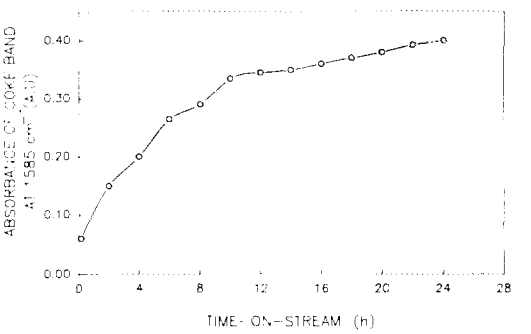

FIG. 7. Coke formation during the cracking of cumene over MAPO-36 at 673 K.

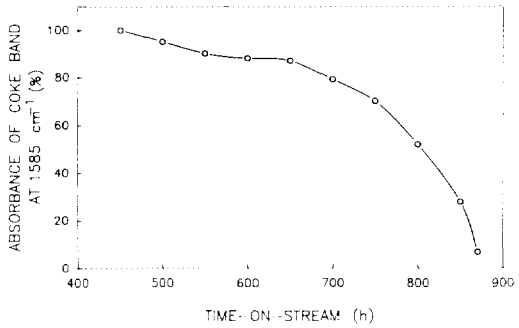

FIG. 8. Temperature programmed oxidation of coke deposited during the cumene cracking over MAPO-36.

After 120 min of the cumene reaction, a novel band appeared at around 1540 cm^{-1}, ascribed to polynuclear aromatic compounds (*23*). With the reaction period, the coke band at 1540 cm^{-1} became more intense than the coke band at 1585 cm^{-1}. The formation of coke increases as a function of time-on-stream and maximum coke formation (86%) occurs in the reaction period of 10 h; later the coke formation is slowed down.

Investigation of coke removal from the deactivated MAPO-36 was studied by temperature programmed oxidation (TPO) and simultaneously monitoring the IR band at 1585 cm^{-1}. Figure 8 shows the temperature programmed oxidation of coke deposited during the cumene cracking reaction over MAPO-36. The initial rate of coke oxidation is low up to 673 K. In the temperature range of 453–673 K (step 1), the removal of coke (which is approximately 15%) is due to the oxidation of sorbed or occluded carbonaceous products near the pore mouth (pore opening) and on the external crystallite surface.

Further, the rate of oxidation of coke increases in the temperature ranges 673–750 K (step 2) and 750–875 K (step 3), respectively. In this temperature ranges of 673–750 K and 750–875 K, the extent of coke removed by oxidation was 20% and 60%, respectively. In these temperature ranges, the coke removal (i.e., oxidation of coke) is faster than in the initial temperature range (453–673 K). This is because of the fact that coke removal by combustion is autoactivated as the temperature increases. The remaining 5% of coke could not be removed at 875 K. This type of coke is carbonaceous residue/microcrystalline graphitic carbon. This indicates that highly graphitic carbon experiences combustion with difficulty. The presence of a small amount of carbonaceous residue even at 875 K indicates that it is sorbed very strongly on some of the strong acid sites. This result is in agreement with the cumene cracking activity of the regenerated MAPO-36, which was restored to 97% only. The decrease in the catalytic activity of the regenerated MAPO-36 compared to that of fresh MAPO-36 is because of the deactivation of some of the acid sites due to the deposition of carbonaceous residue. The results of the TPO of coke deposited over MAPO-36 are qualitative and demonstrate the technique.

CONCLUSIONS

MAPO-36 shows higher catalytic activity and aromatics formation in ethanol, *n*-hexane, cyclohexane, and isooctane conversion reactions than MAPO-5, SAPO-5, and $AlPO_4$-5. The aliphatics and aromatics distributions are different in these reactions over MAPO-36, MAPO-5, SAPO-5, $AlPO_4$-5, and H-ZSM-5. In the *n*-hexane conversion reaction, H-ZSM-5 exhibited higher catalytic activity and lower aromatic formation than MAPO-36. The trend is reversed in cyclohexane conversion reaction.

The toluene disproportionation and *o*-xylene conversion activity of MAPO-36 is very high among the other catalysts. Selective poisoning of the strong acid sites of the catalysts decreased toluene conversion, which indicates the involvement of strong acid sites in the reaction. Pyridine poisoning increases the paraselectivity. In the *o*-xylene conversion reaction, MAPO-36 showed the highest xylene loss, indicating that the disproportionation is more pronounced than the isomerization.

Comparison of catalytic performance be-

tween MAPO-36 and MAPO-5 (both containing similar framework compositions but having different crystal structures) in the hydrocarbon and alcohol reactions revealed that MAPO-36 is more catalytically active. The higher catalytic activity of MAPO-36 than of MAPO-5, SAPO-5, and $AlPO_4$-5 is due to the presence of stronger acid sites.

The catalytic activity of MAPO-36 varies significantly in the conversion of *n*-pentane, *n*-hexane, 3-methyl pentane, cyclohexane, methanol, toluene, and ethylbenzene and it decreases as a function of pulse number due to coke deposition. In the ethylbenzene conversion reaction, MAPO-36 was less deactivated as compared to the type 5 aluminophosphates. The results for the dependence of cumene activity of MAPO-36, SAPO-5, and $AlPO_4$-5 on time-on-stream indicate that MAPO-36 exhibits initial high activity, but this decreases faster than that of SAPO-5 and $AlPO_4$-5. The decrease in the catalytic activity is due to coke deposition in the unidimensional channels and the external crystallite surface. Micropore volume measurements of the uncoked and coked MAPO-36 revealed that the coke formed during the cracking of cumene is deposited in the micropores and occupies 13% of the micropore volume. Regenerated MAPO-36 regained its initial cumene cracking activity to a large extent.

The overall results indicate that MAPO-36 stands high with respect to catalytic activity among MAPO-5, SAPO-5, and $AlPO_4$-5. The large differences in the acidity, pore size, degree of pore constraint, channel system, and structure of the aluminophosphates of type 36 and 5 and pentasil zeolite are responsible for the different catalytic activity and the distribution of aliphatics and aromatics.

ACKNOWLEDGMENTS

The author is sincerely thankful to Dr. H. G. Karge of the Fritz Haber Institute of the Max Planck Society, Berlin, Germany for providing the experimental facilities and helpful discussions. The author is grateful to the Alexander von Humboldt Foundation, Bonn, Germany for an award of an international research fellowship.

REFERENCES

1. Flanigen, E. M., Lok, B. M., Patton, R. L., and Wilson, S. T., *in* "Proceedings, 7th International Zeolite Conference, Tokyo, 1986" (Y. Murakami, A. Lijima, and J. W. Ward, Eds.), p. 103. Kodansha, Tokyo, 1986.
2. Smith, J. V., Pluth, J. J., and Andries, K. J., *in* "Atlas of Zeolite Structure Types" (W. M. Meir, and D. H. Olson, Eds.), 3rd revised ed., p. 50. Butterworth–Heinemann, London, 1992.
3. Akolekar, D. B., *Zeolites*, in press.
4. Akolekar, D. B., *J. Catal.* **143,** 227 (1993).
5. Wilson, S. T., and Flanigen, E. M., *ASC Symp. Ser.* **398,** 329 (1989).
6. Wilson, S. T., Lok, B. M., Messina, C. A., Cannan, T. R., and Flanigen, E. M., *J. Am. Chem. Soc.* **104,** 1146 (1982).
7. Akolekar, D. B., "Sorption, Diffusion and Catalytic Reactions on Zeolites and Zeolite-like Materials." Ph.D. thesis, University of Poona, Poona, 1987.
8. Nayak, V. S., and Choudhary, V. R., *Appl. Catal.* **4,** 333 (1982).
9. Karge, H. G., *Z. Phys. Chem.* **122,** 103 (1980).
10. Karge, H. G., and Boldingh, E. P., *Catal. Today*, **3,** 53 (1988).
11. Derouane, E. G., Dejaifve, P., Gabelica, Z., and Vedrine, J. C., *Faraday Discuss. Chem. Soc.* **72,** 331 (1981).
12. Harrison, I. D., Leach, H. F., and Whan, D. A., *in* "Proceedings 6th International Zeolite Conference, Reno, 1983" (D. H. Olson and A. Bisio, Eds.), p. 479.
13. Harrison, I. D., Leach, H. F., and Whan, D. A., *Zeolites* **7,** 21 (1987).
14. Haung, M., and Kaliaguine, S., *J. Mol. Catal.*, in press.
15. Choudhary, V. R., and Akolekar, D. B., *J. Catal.* **125,** 143 (1990).
16. Guisnet, M., Cormerais, F. X., Chen, Y. S., Perot, G., and Freund, E., *Zeolites* **4,** 108 (1984).
17. Theoduru, D., and Wei, J., *J. Catal.* **83,** 205 (1983).
18. Barrer, R. M., *Adv. Chem. Ser.* **102,** 1 (1971).
19. Choudhary, V. R., and Akolekar, D. B., *J. Catal.* **103,** 115 (1987).
20. Karge, H. G., and Ladebeck, J. P., *Zeolites* **2,** 179 (1982).
21. Eberly, P. E., Jr., *J. Phys. Chem.* **71,** 1717 (1967).
22. Haldeman, R. G., and Botty, M. C., *J. Phys. Chem.* **63,** 489 (1959).
23. Fetting, F., Gallei, E., *Ger. Chem. Eng.* **7,** 32 (1984).